

Interstellar absorptions and shocked clouds towards supernova remnant RX J0852.0-4622^{*}

Yu. V. Pakhomov,¹ N. N. Chugai¹ and A. F. Iyudin^{2,3}

¹*Institute of Astronomy, Russian Academy of Sciences, Pyatnitskaya 48, 119017, Moscow, Russian Federation*

²*Skobeltsyn Institute of Nuclear Physics, Moscow State University, Vorob'evy Gory, 119992 Moscow, Russian Federation*

³*Max-Planck-Institut für Extraterrestrische Physik, Postfach 1312, D-85741 Garching, Germany*

8 March 2013

ABSTRACT

We present results of survey of interstellar absorptions towards supernova remnant (SNR) RX J0852.0-4622. The distribution of K I absorbers along the distance of the background stars is indicative of a local region ($d < 600$ pc) strongly depopulated by K I line-absorbing clouds. This fact is supported by the behavior of the interstellar extinction. We find four high-velocity Ca II components with velocities of $> 100 \text{ km s}^{-1}$ towards three stars and identify them with shocked clouds of Vela SNR. We reveal and measure acceleration of two shocked clouds at the approaching and receding sides of Vela SNR along the same sight line. The clouds acceleration, velocity, and Ca II column density are used to probe cloud parameters. The total hydrogen column density of both accelerating clouds is found to be similar ($\sim 6 \times 10^{17} \text{ cm}^{-2}$) which indicates that possibly there is a significant amount of small-size clouds in the vicinity of Vela SNR.

Key words: ISM: clouds – ISM: kinematics and dynamics – ISM: lines and bands – ISM: supernova remnants – ISM: structure

1 INTRODUCTION

Optical absorption spectroscopy is a classical tool to probe interstellar (IS) clouds, viz., velocities, Doppler broadening, column density of atomic and molecular species, and temporal variations (Danks & Sembach 1995; Crawford 2003). The direction of Vela SNR is unique among other regions of sky in one important respect: apart from usual low-velocity absorption components we see there fast-moving absorbers with velocities $100\text{--}200 \text{ km s}^{-1}$ (Wallerstein & Silk 1971; Danks & Sembach 1995; Cha & Sembach 2000). These components are identified with IS clouds shocked in the blast wave of Vela SNR. An exciting feature of these high-velocity components is their temporal variability (Danks & Sembach 1995; Cha & Sembach 2000). Among these variations of particular interest is the evidence of cloud acceleration (Cha & Sembach 2000) which probably reflects ongoing process of blast wave/cloud interaction in Vela SNR. Surprisingly enough, no attempts have been made so far to utilise acceleration of shocked clouds as an important observational constraint of cloud parameters.

Recently, we performed low- and high-resolution spectroscopic survey of 14 stars in the field of RX J0852.0-4622 aka Vela Jr. The latter is superimposed on the south-east

part of the Vela SNR. The analysis of low-resolution observations in the region $3700\text{--}4000 \text{ \AA}$ was reported earlier (Iyudin et al. 2010). Here we address the high resolution spectral data which cover much broader spectral range. We find the results of analysis of these spectra are of great interest by several reasons. Firstly, our survey covers poorly observed region of Vela SNR. Only two stars HD 75309 and HD 75821 of the previous survey (Cha & Sembach 2000) fall into this region. Secondly, our spectra cover essentially larger spectral range than any other previous survey in the Vela direction. This permits us to obtain more extensive picture of interstellar atomic and molecular absorbers in the Vela SNR direction. Thirdly, and most importantly, HD 75309, the common star of our and Cha & Sembach (2000) survey, shows high-velocity Ca II absorption at -120 km s^{-1} and $+120 \text{ km s}^{-1}$ presumably associated with shocked clouds. Our data combined with those of Cha & Sembach (2000) survey cover large time interval of 15 yr which open up a possibility to measure rather precisely the velocity change of shocked clouds, and thus to recover the clouds acceleration. In turn, the cloud acceleration value in combination with the velocity and Ca II column density provides us with a new diagnostic tool for probing cloud parameters.

The paper is organized as follows. We first describe observations and the extraction of interstellar lines (Section 2). In two cases the stars turn out slow rotators and, therefore, detailed stellar atmosphere analysis is used to recover inter-

^{*} Based on observations collected at the European Southern Observatory, Chile, 080.D-0012(A)

Table 1. List of observed stars

Star	RA		Decl	m_v (mag)	SpType	$(B - V)$ (mag)	A_V (mag)	d (pc)	S/N			
	(eq. 2000.0)								all	Ca II	Na I	K I
HD 75309	08 47 28.0	-46 27 04	7.84	B2Ib/II	0.01	0.8	1900±300	113	38	146	114	
HD 75820	08 50 26.0	-46 14 53	8.64	B9V	-0.02	0.2	470±100	79	30	101	78	
HD 75873	08 50 48.8	-46 18 36	8.10	A3II/III	0.38	1.2	1400±200	67	18	88	82	
HD 75955	08 51 26.0	-45 37 23	7.73	B9V	-0.01	0.2	320± 70	65	20	83	61	
HD 75968	08 51 32.8	-46 36 36	8.14	B9III/IV	-0.12	0.0	570±140	45	14	61	57	
HD 76060	08 52 02.4	-46 17 20	7.88	B8IV/V	-0.09	0.1	390± 90	101	34	130	97	
HD 76589	08 55 23.0	-46 53 28	8.34	B9IV	-0.05	0.1	390± 90	67	17	87	66	
HD 76649	08 55 50.4	-46 20 30	8.33	B7II/III	0.14	0.8	640±110	57	14	74	65	
HD 76744	08 56 18.2	-46 19 57	8.69	A0V	0.08	0.5	270± 50	61	18	78	59	
CD-454590	08 49 35.5	-46 23 18	9.58	B5	0.20	1.3	2400±300	41	11	53	43	
CD-454606	08 50 15.0	-45 31 22	8.96	B0.5V	0.38	2.0	1670±160	63	18	82	72	
CD-454645	08 51 34.9	-46 09 54	10.32	A0	0.20	0.4	330± 70	38	11	49	41	
CD-454676	08 53 22.0	-46 02 09	8.93	B0.5III	0.77	3.2	1080±150	38	13	52	54	
CD-464666	08 50 44.3	-46 38 11	9.81	A0II	0.60	2.1	5700±500	37	12	50	51	

stellar absorption. The parameters of interstellar absorption components and their analysis are presented in Section 3. In Section 4 we address the shocked clouds in the sight line of HD 75309. The cloud acceleration, velocity and Ca II column density are used for probing cloud parameters on the bases of cloud shock model in which we include all the relevant physics.

2 OBSERVATIONS AND DATA REDUCTION

The spectra of 14 stars in direction of Vela Jr. [for star position see (Iyudin et al. 2010)] were obtained in March 2008 on the 3.6-m ESO NTT telescope equipped with EMMI spectrograph (echelle grating #14, cross-dispersion grating #3, CCD mosaic 2076x4110). The full coverage is 3850-8620 Å with the gap at 5570-5650 Å; the central dispersion is 0.02 Å/pix, the resolving power is $R = \lambda/\Delta\lambda = 88\,600$ ($\Delta v = 3.4$ km s⁻¹). In Table 1 stars are listed with their HD/CD name, equatorial coordinates, V -magnitude, spectral type, $B - V$ color, and signal-to-noise ratio (S/N), average and at Ca II 3933, 3968 Å, Na I 5889, 5895 Å, and K I 7664, 7698 Å positions. Preliminary processing of CCD images, spectra extracting, wavelength calibration with ThAr lamp, normalizing and merging of orders is performed using *echelle* package of *MIDAS*. In order to normalize the spectra a blaze function of the echelle is recovered using a calibrated flux of the standard star HD 60753. Its stellar flux is synthesized by applying *ATLAS9* code (Kurucz 1993) and *SynthVb* (Tsybal et al. 2003). A stellar atmosphere model of standard star is calculated for the solar metallicity with parameters $T_{eff} = 16200$ K, $\log g = 3.56$, $V \sin i = 24$ km s⁻¹, and interstellar absorption $A_V = 0.25$ (Iyudin et al. 2010).

For most stars we used stellar synthetic spectrum assuming solar element abundances because these objects belong to the thin disk of Galaxy. We find that small deviations ($\lesssim 0.3$ dex) from the solar abundance do not affect the extracted interstellar lines, if the stellar rotation is high ($\gtrsim 30$ km s⁻¹). In case of star HD 75873 the rotation is slow, $V \sin i = 3$ km s⁻¹, and, therefore, a stellar synthetic spectrum with carefully determined chemical composition should be used to extract interstellar lines. A similar procedure is applied to CD-464666.

The stellar parameters of HD 75873 are found by employing a standard requirement that the chemical composition should be stable against variations of the line excitation potential and ionization state. The *ATLAS9* code is used to derive parameters of the stellar atmosphere and *WIDTH9* (Kurucz 1993) for the abundance determination. The stellar parameters inferred in this way ($T_{eff} = 8900$ K, $\log g = 2.50$) are consistent with those determined earlier using only hydrogen lines (Iyudin et al. 2010). The microturbulent velocity ($V_t = 2.5$ km s⁻¹) is derived using requirement that the Fe/H ratio should not depend on the intensity of Fe II lines. The recovered element abundance slightly exceeds the solar value; the Fe overabundance is $+0.08 \pm 0.11$ dex. In case of CD-464666, most distant star of the program, we find $T_{eff} = 10100 \pm 300$ K, $\log g = 2.0 \pm 0.2$, and $V_t = 2.5 \pm 0.5$ km s⁻¹. The distance we infer using the spectral parallax method is 5800 ± 900 pc, in agreement with the previous estimate 5700 ± 500 pc (Iyudin et al. 2010). The inferred element abundance is close to the solar one; Fe overabundance is of $+0.05 \pm 0.11$ dex.

The extracted spectrum of the interstellar absorption (Fig. 1) is represented by a residual flux

$$F(\lambda) = 1 - (F_{syn}(\lambda) - F_{obs}(\lambda))/F_{cont}(\lambda),$$

where F_{obs} is the observed normalized flux of the stellar spectrum, F_{syn} is the model normalized flux calculated using *SynthV* package and VALD line list (Kupka et al. 1999), F_{cont} is the continuum flux. We extracted telluric lines in case of Na I 5895 Å, K I 7664 Å, and diffuse interstellar bands (DIBs).

3 DATA ANALYSIS

3.1 Overview of IS absorptions

The interstellar spectra show absorption lines of Ca II 3933, 3968 Å, Na I 5889, 5895 Å, K I 7664, 7698 Å, CH 4300 Å, CH⁺ 4232 Å, and DIBs. The Ca I 4226 Å line is not detected, in accord with the well known weakness of this line (Welty et al. 2003). In Fig. 2 we present a zoom of Na I, Ca II, K I, CH, and CH⁺ interstellar lines for the interesting case of HD 75309 ($d = 1900$ pc) showing high-velocity

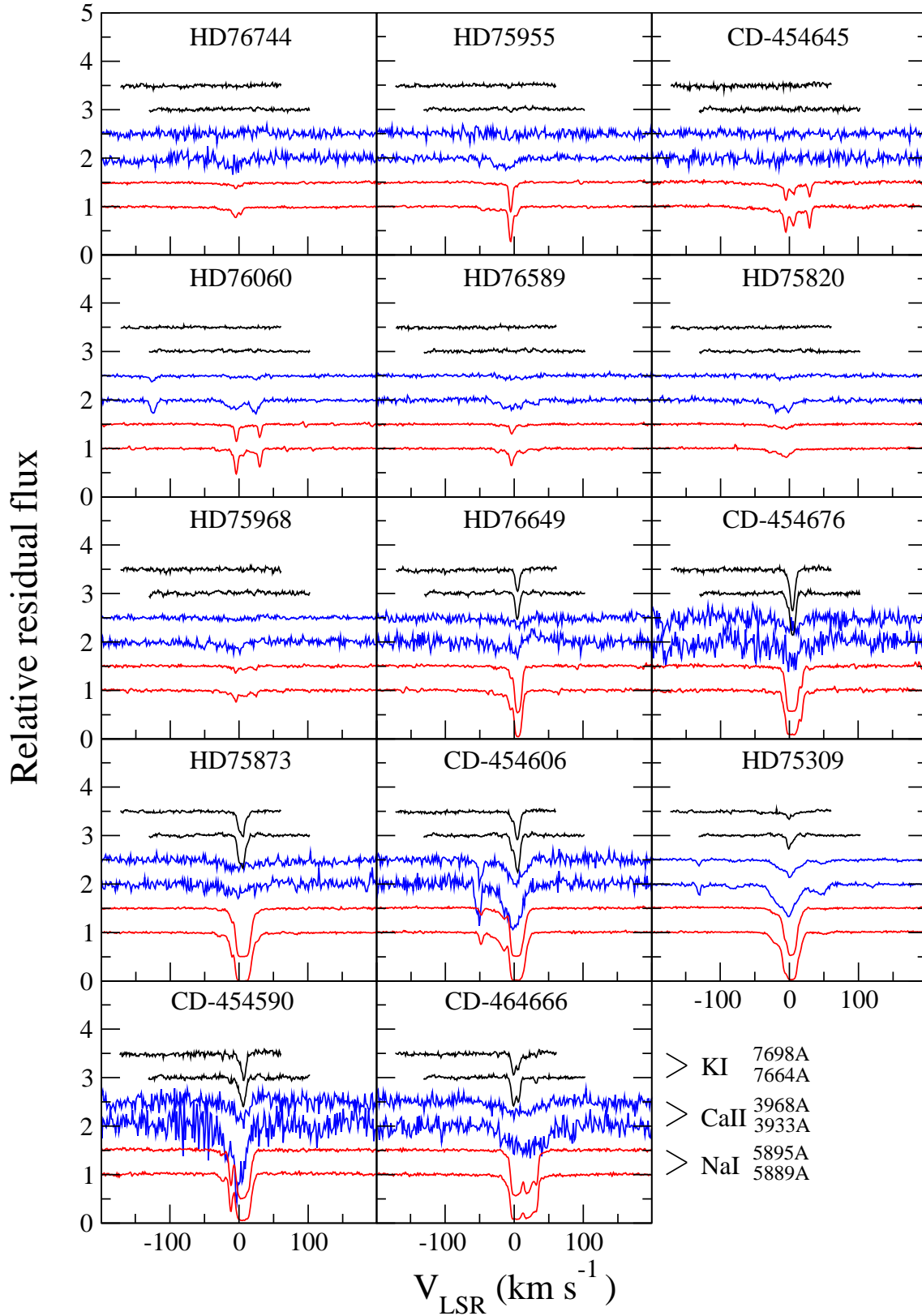


Figure 1. Interstellar absorption lines of K I, Ca II, and Na I in spectra of program stars. The star distance increases from left to right and from top to bottom. In the right-bottom corner we show position of spectral lines. All continuum fluxes are normalized to unity. Spectra are shifted in vertical direction for convenience.

Table 2. Equivalent widths (mÅ) of interstellar atomic and molecular lines

Star	Ca II		Na I		K I		CH	CH ⁺
	3933 Å	3968 Å	5889 Å	5895 Å	7664 Å	7698 Å	4300 Å	4232 Å
HD 75309	297	131	567	450	57	52	6	7
HD 75820	96	16	110	50	—	—	—	—
HD 75873	101	100	536	454	204	161	26	10
HD 75955	87	21	199	116	—	—	—	—
HD 75968	62	17	122	74	—	—	—	—
HD 76060	108	22	192	110	—	—	—	—
HD 76589	85	28	115	63	—	—	—	—
HD 76649	41	65	383	283	82	89	15	8
HD 76744	77	—	101	50	—	—	—	—
CD-454590	431	113	568	533	164	132	22	20
CD-454606	368	189	632	496	198	153	22	11
CD-454645	17	10	244	169	—	—	—	—
CD-454676	156	107	470	427	228	208	37	6
CD-464666	283	147	780	694	177	136	6	17

Table 3. Equivalent widths (mÅ) of DIBs

Star	5780 Å	5797 Å	5850 Å	6196 Å	6203 Å	6270 Å	6284 Å	6376 Å	6379 Å	6614 Å	6660 Å	7224 Å
HD 75309	143	20	—	11	43	26	308	—	16	52	10	31
HD 75820	—	—	—	—	—	—	—	—	—	—	—	—
HD 75873	321	75	25	29	73	62	598	16	41	118	24	56
HD 75955	—	12	—	—	—	—	—	—	—	—	—	—
HD 75968	23	—	—	—	—	—	27	—	—	—	—	—
HD 76060	22	—	—	—	—	—	24	—	—	—	—	—
HD 76589	18	—	—	—	—	—	—	—	—	—	—	—
HD 76649	114	27	—	—	19	—	253	—	11	—	—	—
HD 76744	10	—	—	—	—	—	—	—	—	—	—	—
CD-454590	246	97	18	27	62	47	620	15	54	107	30	65
CD-454606	261	74	21	24	57	41	409	18	46	128	21	44
CD-454645	—	—	—	—	—	—	63	—	—	—	—	—
CD-454676	334	134	35	30	82	37	769	20	71	151	21	86
CD-464666	485	125	30	35	113	59	966	23	58	161	33	94

($|v| > 100 \text{ km s}^{-1}$) Ca II components that will be addressed below. Total equivalent widths of the detected interstellar absorptions are given in Table 2.

The interstellar Na I doublet is detected in the spectra of all stars (Fig. 1). This line, as expected, becomes stronger as star distance increases. In most cases Ca II doublet is significantly weaker than that of Na I which is well known fact and usually explained as an effect of a strong Ca depletion onto dust grains. K I doublet is seen only in stars with large extinction and strong molecular absorptions of CH and CH⁺. The equivalent width of K I 7698 Å absorption tightly correlates with the total equivalent width of molecular lines of CH and CH⁺. (Table 2). This correlation agrees with the strong correlation between K I and CN column densities (Welty & Hobbs 2001).

The spectra arranged according to the star distance in Fig. 1 reveal a striking behavior of K I absorptions: they are not detected for stars with distances $d < 600 \text{ pc}$ ($N(\text{K I}) < 5 \times 10^{10} \text{ cm}^{-2}$) and then sharply get strong for stars with distances $d > 600 \text{ pc}$ (Fig. 3,a). The "jump" in the distribution of K I absorbers along the distance is indicative of a "cavity" in the region $d < 600 \text{ pc}$ underpopulated by cool clouds. This conjecture is supported by a similar

behavior of the interstellar extinction although in this case the threshold effect is not as strong as for K I absorbers (Fig. 3,b).

Twelve diffuse interstellar bands are detected in our sample and listed in Table 3. Empty place in the table indicates that this particular DIB is absent or its equivalent width is smaller than 10 mÅ. Most DIBs with $\lambda < 5500 \text{ Å}$ cannot be extracted because of low S/N ratio. In an extensive survey of DIBs in spectra of ~ 200 stars (Friedman et al. 2011) finds a strong correlation of equivalent widths (W in mÅ) of 6284 Å and 5780 Å DIBs (correlation coefficient $r = 0.96$) with the linear fit $W(6284) = a + bW(5780)$, where $a = 28.24 \pm 5.8$ and $b = 2.32 \pm 0.03$. In our small sample the correlation even stronger ($r = 0.99$), while the parameters of the linear fit are a bit different: $a = 1.5 \pm 46$ and $b = 2.03 \pm 0.18$. Yet the relatively small value of a term in our case seems to be more easy to conform with the expected zero value of W in case of vanishing molecular abundance.

3.2 Component parameters

Crawford (2001) demonstrated upon the bases of high-

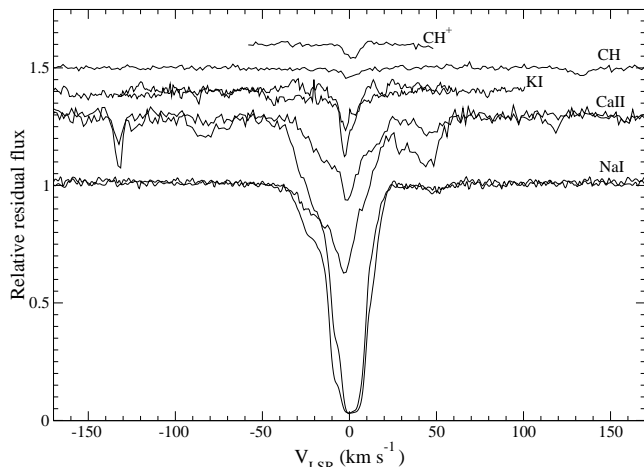


Figure 2. Interstellar absorption lines in spectra of HD 75309. All continuum fluxes are normalized to unity. Spectra are shifted in vertical direction for convenience.

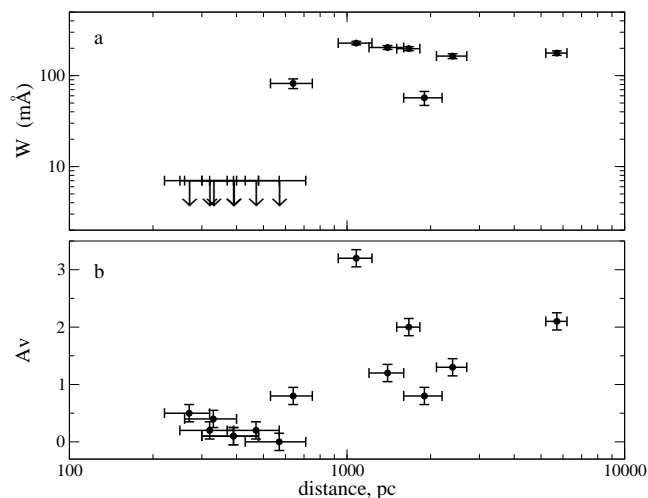


Figure 3. Equivalent width of KI absorption (*upper panel*) and extinction (*lower panel*) vs. star distance. Arrows in upper panel show upper limits.

resolution ($\Delta v \approx 0.3 \text{ km s}^{-1}$) observations that Doppler parameters of interstellar line components lie in the range of $0.3 \leq b \leq 2.2 \text{ km s}^{-1}$. Our spectra have lower resolution ($\Delta v = 3.4 \text{ km s}^{-1}$) so most of the interstellar line components are expected to be unresolved. This precludes reliable determination of the Doppler parameter of a single line. Fortunately, in cases of Na I, Ca II, and KI we have in hand a doublet ratio; this provides us with the additional relation which permits one to recover both N and b even for unresolved lines. Generally, the blend of M components is decomposed using standard relations

$$F(v) = (e^{-\tau(v)} * \Theta) \quad (1)$$

$$\tau(v) = \sigma_0 f \lambda \sum_{k=1}^M N_k \phi\left(\frac{v - v_k}{b_k}\right), \quad (2)$$

where the first equation is a convolution of the line profile with the instrumental profile Θ . In the second equation $\sigma_0 = 0.0265$ is the integrated cross-section param-

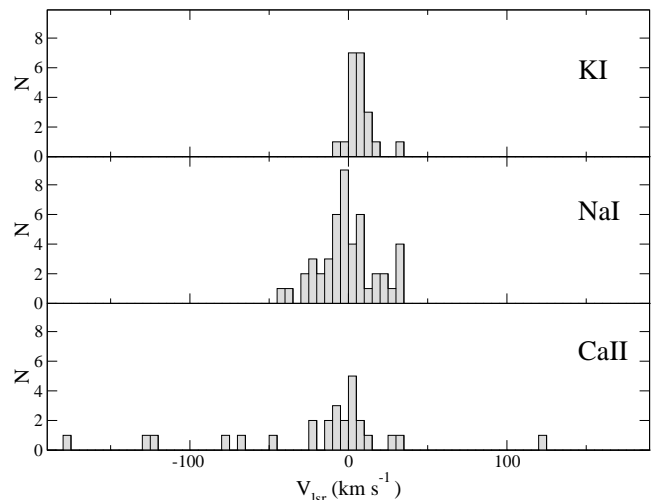


Figure 4. Velocity distribution of resolved components of interstellar absorptions of KI, Na I, and Ca II.

ter, f is the oscillator strength taken from VALD database (Kupka et al. 1999) for atomic lines and from Gredel et al. (1993) for molecular lines, N_k is the column density of k -th component, and $\phi(u/b) = (1/b\sqrt{\pi}) \exp(-u^2/b^2)$ is the Gaussian velocity distribution of an absorbing gas in a cloud along the sight line.

Parameters of interstellar absorption components derived by the minimization procedure are listed in Table 4. The radial velocity is reduced to the local standard of rest (LSR) using the Sun velocity towards Vela Jr. $\Delta v_{\text{LSR}} = -15.7 \text{ km s}^{-1}$ (Famaey et al. 2005). For each atomic species three columns (v_{LSR} , b , and N) are given. The Doppler parameter for molecular lines is omitted because it cannot be reliably determined. Data with the large errors are marked by the colon. The typical v_{LSR} error is $0.1\text{--}0.2 \text{ km s}^{-1}$ ($0.5\text{--}1 \text{ km s}^{-1}$ in case of the low accuracy), b error is $0.1\text{--}0.4 \text{ km s}^{-1}$ ($1\text{--}1.5 \text{ km s}^{-1}$ in case of the low accuracy); for N a typical relative error is 10% and 30% in case of the low accuracy. The blends with unresolved saturated lines are marked by italic with the estimated velocities shown in parentheses.

The average Na I column density of components in our sample ($3.5 \times 10^{11} \text{ cm}^{-2}$) is larger compared to $1.2 \times 10^{11} \text{ cm}^{-2}$, the average value for the high-resolution survey of Welty et al. (1994). We attribute this disparity to the low resolution of our spectra which leads to the omission of the significant number of thin cloud components in absorption blends. This effect is apparent also in the velocity distribution (Fig. 4). KI absorptions are rather weak so the components are recovered confidently. The velocity dispersion of KI absorbers $\sigma_v \approx 8 \text{ km s}^{-1}$ is the same as the value 7.8 km s^{-1} found for an extensive survey for KI components with $\log N < 11.3 \text{ cm}^{-2}$ (Welty & Hobbs 2001). For stronger components these authors find somewhat lower value $\sigma_v = 5.8 \text{ km s}^{-1}$. Our small sample precludes more refined analysis of the velocity distribution of strong KI components. In case of Na I the velocity distribution (Fig. 4) is rather broad with $\sigma_v \approx 18 \text{ km s}^{-1}$, twice as large compared to $\sigma_v \approx 9 \text{ km s}^{-1}$ found by Welty et al. (1994) in an extensive survey of the Na I IS absorption. The striking disparity is caused probably by the relatively low resolution and S/N

Table 4. Parameters of the resolved components of interstellar absorptions

Star	Ca II			Na I			K I			CH		CH+	
	v_{lsr} (km s ⁻¹)	b (km s ⁻¹)	N_{11} (cm ⁻²)	v_{lsr} (km s ⁻¹)	b (km s ⁻¹)	N_{11} (cm ⁻²)	v_{lsr} (km s ⁻¹)	b (km s ⁻¹)	N_{11} (cm ⁻²)	v_{lsr} (km s ⁻¹)	N_{11} (cm ⁻²)	v_{lsr} (km s ⁻¹)	N_{11} (cm ⁻²)
HD 75309	-127.1 -77: -65: -28...25(-22: -9: 2.5: 12.5:) 33...55 123.9	1.6 2: 1.5: 2.0	2.0 1: 0.5: 3.0	-17: -2.6 2...11(5.0: 8.8:) 20: 3:		3:	2.7 8.6	1.5 2.0	1.5 0.6	5.0: 75:		6.6 96	
HD 75820	-14.9 2.0		3.0: 3.0	-27.1: -22.2: -13.6: -7.6: -1.0 4.5 8.2	1.0: 1.0: 1.5 1.0: 1.1 1.0: 1.0:	0.5: 0.5: 0.6: 0.9: 1.1: 0.5: 0.4:							
HD 75873	1.4:		13:	-25.6 -6.8 -3...25 30.2	3.0: 2.3: 3.0:	0.6 4.8: 1.5:	3.2 9.1 15.4	1.5 1.5 0.7:	4.4 7.6 1.1	4.5: 400:		6.1 158	
HD 75955	-21: -3:		3.5 5.5	-39.2 -19.3 -1.1 7.5	1.4 1.3 1.4 1.7	0.4: 0.5: 16.5 1.2							
HD 75968	1.0:		6.0:	-12.8 -6.7 -1.6 10.8 27.2	1.0: 1.5: 1.0 1.5: 0.5:	0.4 0.4 1.7 0.7 0.8							
HD 76060	-121.8 -15...7(-8: -1:) 26.4:	4: 7:	4: 6.3:	-0.8 9.1 33.2	1.5 2.5: 0.9	5.6 1.0: 3.9							
HD 76589	-27...13 35:		-21.1 1.4:	2.0 -7.5 -1.2 3.8 16.1	0.5 1.5 1.4 0.7 3.5	0.5: 2.6 0.8: 0.7							
HD 76649				-2.2 1...16	1.3	3.8	6.9 10.6	1.0: 0.3:	6.7: 1.5:	8.1 220		8.0 130	
HD 76744	-5.0:			-22...-15 -6.5 -1.7 5.2	1.9 1.5 2.6	0.6 1.2 1.0							
CD-454590	-15...17(-13.5: 2: 9:)			-20.2 -7.8 -2...27	2.5 1.3	1.2 50	-8.0 -1.4 4.6 6.7 10.5 14.4	0.8 0.7: 0.8: 0.6: 0.6: 0.6:	0.7: 0.7: 0.7: 1.1: 29: 1.3	3.1: 11.2	85: 280	8.0 290	
CD-454606	-46.2: -14...25	3.5	19:	-43.6 -10.1 -3...28	1.0 1.0	1.8 3.3	1.6 9.2	2.2 2.5	1.9 9.1	3.4 9.5	111 223	6.6 120	
CD-454645				-1.8 8.9 32.6	1.2 3.0 1.1	5.5 3.4 3.9							
CD-454676	-177.3: 6:		8:	-8...16 20.1 33...38	1.6	7.9	0...12(0.4: 1: 7.5)			7.2 580		8.8 135	
CD-464666	-25...50			-3...38(1: 21: 35:)			2.2 9.2 34.7	1.3 2.2 0.7	6.0 3.7 0.6	4.8 32:		6.7	

of our spectra which precludes decomposition of saturated blends of Na I absorptions. As a result we strongly underestimate the number of low-velocity components of Na I.

The large velocity dispersion of Ca II absorption components (Fig. 4) stems from two effects. The first is the same selection effect as in case of Na I absorption, while the second effect is the well known phenomenon discussed Routly & Spitzer (1952): the larger ratio $N(\text{Ca II})/N(\text{Na I})$ for components with higher velocity. A standard explanation of the Routly-Spitzer effect is the dust destruction in the dynamically disturbed clouds which results in release of gaseous Ca. The fact that we see high-velocity components in Ca II lines and not in Na I lines indicates that high-velocity clouds have low neutral hydrogen column density in which case the equivalent width of Na I absorption turns out below the detection limit of our data.

In some cases positive velocities of $v_{\text{lsr}} < 50 \text{ km s}^{-1}$ are related with a velocity gradient caused by the galactic rotation. For the most distant star CD-464666 ($d = 5700 \text{ pc}$) adopting galactocentric distance of 8.5 kpc and Galaxy rotational velocity of 220 km s^{-1} we find that Galactic rotation can be responsible for the positive LSR velocities in the range of $v \leq 50 \pm 4 \text{ km s}^{-1}$. Remarkably, this value is consistent with the upper limit of the observed velocity interval of the Ca II absorption ($-25 \dots +50 \text{ km s}^{-1}$) towards CD-464666.

Two nearest stars of our sample, CD-454645 ($d = 330 \pm 70 \text{ pc}$) and HD 76060 ($d = 335 \pm 63 \text{ pc}$), show a strong Na I component with similar velocity (32.6 km s^{-1} and 33.2 km s^{-1}), Doppler parameter (1.1 km s^{-1} and 0.9 km s^{-1}), and column density ($3.9 \times 10^{11} \text{ cm}^{-2}$). This suggests that we see both stars through the same IS cloud. For the distance of $\approx 330 \text{ pc}$ the angular separation θ' between these stars corresponds to the linear scale of 0.85 pc. We conclude therefore that the tangential size of this cloud $\gtrsim 1 \text{ pc}$. The large LSR velocity (33 km s^{-1}) indicates that this cloud belongs to the dynamically disturbed ISM. Remarkably, however, that we do not detect similar component in Ca II suggested by Routly-Spitzer effect. This indicated that this fast-moving material contains significant amount dust with the most Ca locked in grains.

Of particular interest are four fast-moving Ca II components (Table 4) with velocities exceeding 100 km s^{-1} in sight lines of three stars, specifically, -177 km s^{-1} (CD-454676), -125 and $+120 \text{ km s}^{-1}$ (HD 75309), and -122 km s^{-1} (HD 76060). Following the earlier conjecture invoked for similar high-velocity components (Wallerstein & Silk 1971; Jenkins et al. 1976; Cha & Sembach 2000) towards Vela SNR we attribute the fast-moving material to the IS clouds shocked by Vela SNR.

Alternatively, high velocity clouds of our survey might be attributed to the SNR RX J0852.0-4622. We consider, however, this possibility unlikely because RX J0852.0-4622 is a young SNR that expands with the velocity of $\sim 10^4 \text{ km s}^{-1}$ (Iyudin et al. 1998; Aschenbach 1998). In this case velocities of shocked clouds unlikely would be the same as in old Vela SNR. The identification of detected high-velocity components with Vela SNR is thus preferred.

Table 5. Evolution of high-velocity components in spectra of HD 75309

Year	cloud A			cloud B		
	v_{lsr} (km s^{-1})	W ($\text{m}\text{\AA}$)	N (10^{11} cm^{-2})	v_{lsr} (km s^{-1})	W ($\text{m}\text{\AA}$)	N (10^{11} cm^{-2})
1993	-121.9 ± 0.3	12 ± 1	1.4 ± 0.1	119.3 ± 0.3	9 ± 1	1.0 ± 0.1
1996	-123.8 ± 0.1	16 ± 1	1.8 ± 0.1	119.9 ± 0.3	7 ± 1	0.8 ± 0.1
2008	-127.1 ± 0.1	16 ± 1	1.8 ± 0.1	123.9 ± 0.1	5 ± 1	0.6 ± 0.1

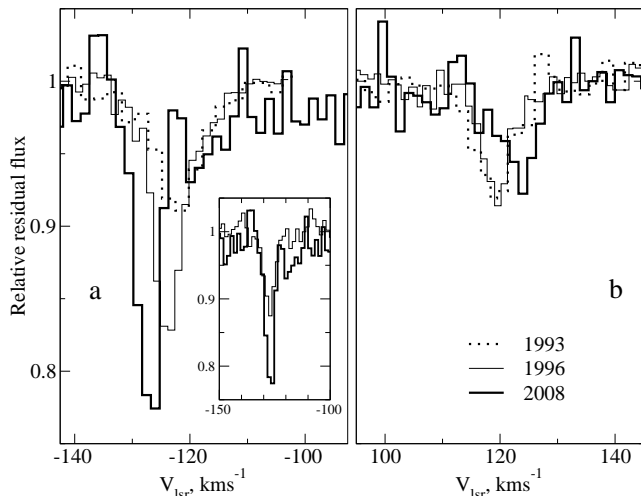


Figure 5. The profiles of Ca II absorption in spectra of star HD 75309 for three epochs. For all the epochs Ca II K are shown. In the inset we show both K (thick) and H Ca II lines in 2008 spectrum to demonstrate that the noise does not affect the narrow component position.

3.3 Acceleration of high-velocity clouds in sight line of HD 75309

Interstellar lines towards HD 75309 were observed in February 1993 and January/February 1996 (Cha & Sembach 2000) with the spectral resolution comparable with that of our data. Authors noticed increase of a column density of Ca II fast component with velocity -120 km s^{-1} but did not mention any velocity variation. We combine their data with our observations to look at the velocity change on the time scale of 12–15 yr. It should be noted that velocities reported by Cha & Sembach (2000) are larger compared to ours by 4 km s^{-1} for all the components. The major part of this difference (2.6 km s^{-1}) is explained by the new value we use for the solar motion (Famaey et al. 2005). The remaining 1.4 km s^{-1} which is comparable with one pixel is unclear but could be related with the wavelength calibration uncertainty of both spectra. Despite this uncertainty the velocity change of the fast components can be measured with high precision via the cross-correlation technique because slow components of interstellar absorption lines remain unchanged. This procedure permits us to establish a common zero point in the velocity space and thus to measure the velocity change over the past period of time.

The high-velocity components of -127 km s^{-1} and $+124 \text{ km s}^{-1}$ according to our data and to those of Cha & Sembach (2000) with the common zero point are

shown in Fig 5. We name the approaching component "cloud A" and receding component "cloud B". The plots clearly demonstrate that both components accelerate. Remarkably, in the case of cloud A both Ca II K and H lines in the 2008 spectrum show similar narrow component thus strengthening the reliability of the velocity determination. Using Gaussian fitting we measure velocity of both clouds at three epochs (Table 5). In the table we give also W and N ; the data on W and N for epochs 1993 and 1995 are taken from Cha & Sembach (2000). The average acceleration between 1993 and 2008 is $-0.33 \pm 0.06 \text{ km s}^{-1} \text{ yr}^{-1}$ for cloud A and $+0.38 \pm 0.06 \text{ km s}^{-1} \text{ yr}^{-1}$ for cloud B. The approaching component seems to change its width while the equivalent width is preserved. The equivalent width of the receding component has noticeably decreased.

The impact parameter (in SNR radius) of the sight line of HD 75309 relative to the Vela SNR center is $p/R \sim 0.5$. Adopting $p/R = 0.5$ and assuming the model of a plane slab perpendicular to the SNR radius we find for the cloud A the deprojected velocity $v_c = 147 \text{ km s}^{-1}$, Ca II column density $N(\text{Ca II}) = 1.6 \times 10^{11} \text{ cm}^{-2}$, and the cloud acceleration $g = 0.38 \text{ km s}^{-1} \text{ yr}^{-1}$ (or $1.2 \times 10^{-3} \text{ cm s}^{-2}$). For the cloud B these values are $v_c = 142 \text{ km s}^{-1}$, $N(\text{Ca II}) = 6.9 \times 10^{10} \text{ cm}^{-2}$, and $g = 0.44 \text{ km s}^{-1} \text{ yr}^{-1}$ (or $1.4 \times 10^{-3} \text{ cm s}^{-2}$). The deprojected values will be used below for the constraining the cloud parameters.

4 PARAMETERS OF SHOCKED CLOUDS

The question we address here is what are the cloud parameters (density and size) which might explain simultaneously the Ca II column density and the acceleration of shocked clouds. Below we rely on the assumption that the interstellar clouds are shocked and accelerated by the blast wave of Vela SNR. We start with the general picture and then use a model of the cloud shock to constrain the cloud parameters.

4.1 General picture

We follow a view that the Vela SNR is the result of an expansion of the Sedov blast wave in the cloudy IS medium (Bocchino et al. 1999). In our estimates and modelling we approximate sub-parsec clouds by a homogeneous sphere which is the idealization for the clumpy cloud. The assumption of a spherical cloud is usually adopted for the analysis of a blast wave/cloud interaction (Klein et al. 1994), particularly in case of a shocked cloud in the Cygnus Loop (Patnaude & Fesen 2005). In fact, since we are interested primarily in the cloud size along the blast wave propagation we do not concern about the clump shape and tangential size. Some justification for the choice of clumpy shape provide 3-dimensional magneto-hydrodynamic simulations (Kritsuk et al. 2011) which demonstrate that initially homogeneous medium evolves towards a two-phase structure in which cool phase grows filamentary but later on the clumpy structure gets dominant. Yet we admit that in some cases a cloud shape may be close to that of a filament or sheet.

A blast wave propagating with the speed v_b in an intercloud medium with the density ρ_{i0} drives a cloud shock wave with the speed $v_s \approx v_b(\rho_{i0}/\rho_{c0})^{1/2}$ (Klein et al. 1994)

where ρ_{c0} is the undisturbed cloud density. (Note, we distinguish between observed cloud velocity v_c and the cloud shock velocity v_s). Adopting the blast wave speed $v_b = 600 \text{ km s}^{-1}$ (Bocchino et al. 1999) and the cloud shock velocity $v_s = 140 \text{ km s}^{-1}$ one finds from the momentum conservation that the cloud-to-intercloud density contrast $\chi \equiv \rho_{c0}/\rho_{i0} \approx (v_b/v_s)^2 \approx 18$. For a typical intercloud density $n_{i0} = 0.1$ (Bocchino et al. 1999) the cloud density is then $n_{c0} \sim 2 \text{ cm}^{-3}$.

The interaction of the blast wave with the cloud of the radius a can be divided roughly into three phases (Klein et al. 1994). At the first stage the cloud shock propagates through the cloud; this stage ends up with the cloud crush in a "cloud crushing time" $t_{cc} = a/v_s$. At the second stage the shocked cloud is accelerated by the dynamical pressure of the blast wave. This is accompanied by the growth of the Kelvin-Helmholtz instability that leads to the cloud fragmentation. The third stage is the final stage of fragmentation which ends up with the full destruction of a cloud and mixing of cloud fragments with the blast wave flow. For the density contrast $10 \leq \chi \leq 100$ the cloud life time is $t_d \sim 4t_{cc}$ (Klein et al. 1994). It should be noted that the shocked cloud may not show acceleration. This would be the case if the time t_{cc} is so large that the cloud has enough time to cross the blast wave before it gets fragmented. The fact that we see the accelerating Ca II line-absorbing gas indicates that the cloud has been already completely shocked and still resides inside the dense part of the blast wave. We however are not able to exactly specify the stage at which the shocked cloud is detected. The conservative statement would be that the accelerating cloud is caught at the stage $t_{cc} < t < 4t_{cc}$ after the interaction between the blast wave and the cloud has turned on.

The cloud acceleration combined with an additional information about Vela SNR can provide us with an estimate of the cloud column density via the equation of a cloud motion driven by the blast wave. For the blast wave postshock velocity of $(3/4)v_b$ and the postshock density of $4n_{i0}$ the equation of the cloud motion reads

$$gN_H = 4n_{i0} \left(\frac{3}{4}v_b - v_c \right)^2, \quad (3)$$

where N_H is the cloud total hydrogen column density normal to the shock plane. Inserting into this equation $g \approx 10^{-3} \text{ cm s}^{-2}$, $v_c = 140 \text{ km s}^{-1}$, $n_{i0} = 0.1 \text{ cm}^{-3}$, $v_b = 600 \text{ km s}^{-1}$ one infers the cloud column density $N_H \approx 5 \times 10^{17} \text{ cm}^{-2}$. This exciting result shows that the accelerated cloud is unlike a typical Na I absorber which is associated with a cloud column density $N_H \sim 8 \times 10^{19} \text{ cm}^{-2}$ (Welty et al. 1994). The derived estimate of N_H combined with the cloud density $n_{c0} \sim 2 \text{ cm}^{-3}$ implies the cloud radius $a = (3/4)N_H/n_{c0} \sim 2 \times 10^{17} \text{ cm}$ assuming initial spherical cloud shape. For this radius the cloud crushing time is $t_{cc} = a/v_c \sim 500 \text{ yr}$.

The above estimates presume a constant dynamical pressure $p_{dyn} = \rho v^2$ of the blast wave. This assumption, however, could easily break down because the dynamical pressure in the blast wave drops downstream rather steeply, $p_{dyn} \propto (r/R)^{11}$ (McKee et al. 1987). Already at $r = 0.97R$ the pressure is $\approx 30\%$ lower compared to the maximum value at the shock front. It is reasonable to adopt the postshock layer $\Delta r \sim 0.03R$ to be the width of the blast wave

in which the dynamical pressure is approximately constant. Because $v_c \ll v_b$, it takes $\Delta t \sim \Delta r/v_b \sim 800$ yr for the cloud in the blast wave frame to cross the blast wave width $\Delta r = 0.03R \approx 0.5$ pc, where we adopt $R = 16$ pc (Cha et al. 1999). The found time scale is only slightly larger than the estimated cloud crushing time $t_{cc} \sim 500$ yr. This has an important implication for the cloud sizes: the initial radius of accelerating clouds cannot significantly exceed 2×10^{17} cm; otherwise the cloud crosses the blast wave before it gets shocked. In this regard it might well be that not all the high-velocity shocked clouds accelerate; some of them might be large enough to cross the blast wave before they get fragmented. These clouds obviously should not experience noticeable acceleration.

4.2 Model outline

The cloud postshock flow will be modelled in a steady plane shock approximation. The major parameters of the shock are the observed cloud shock velocity (v_s), preshock cloud density (n_{c0}), preshock magnetic field (B_0), and preshock hydrogen ionization fraction (x_0). The postshock flow then is determined by a standard set of equations of mass, momentum and energy conservation (Cox 1972). We adopt the parallel frozen-in magnetic field. Cooling function of Sutherland & Dopita (1993) and the low-temperature ($\log T < 3.9$ K) cooling function of Jura & Dalgarno (1972) are used for the cooling rate calculation. We ignore effects of elements depletion onto dust in the cooling function because in the temperature range of interest the cooling function is determined by elements (H, He, C, N, O) which are not affected by the depletion. The hydrogen, helium, Ca, and Na ionization fractions are calculated by solving time-dependent kinetic equations which include radiative recombination, ionization by electron collisions, ionization by the interstellar ultraviolet radiation, by cosmic rays and background X-rays. Among the latter two mechanisms the ionization by background X-rays dominates for small size clouds ($\leq 10^{18}$ cm). We adopt the ionization rate by background X-rays to be $\zeta \approx 7 \times 10^{-16} \text{ s}^{-1}$ (Wolfire et al. 1995). The ionization of Ca II by the recombination Ly γ radiation is also taken into account although this process is of minor importance. Four Ca ions and three Na ions are included in the ionization calculations of these elements.

The interstellar calcium is usually strongly depleted onto dust. We adopt depletion factors $\delta = (\text{Ca}/\text{H})/(\text{Ca}/\text{H})_\odot = 2 \times 10^{-4}$ for Ca and $\delta = 0.1$ for Na (Savage & Sembach 1996). The dust destruction in the shock is treated following standard recipes (Tielens et al. 1994). We take into account the grain acceleration by the betatron mechanism (Shull 1977) and the grain deceleration due to the gas-grain collision. The efficiency of the betatron acceleration is set to be unity, if the grain Larmor radius is small, $r_B(d \ln B/dz) < 1$, and zero otherwise. The major mechanisms of a dust destruction are the grain evaporation in grain-grain collisions, nonthermal grain sputtering by collisions with He, and the thermal dust sputtering (Draine & Salpeter 1979; Tielens et al. 1994). The adopted critical velocity of the vaporization in the grain-grain collision is $v_v = 30 \text{ km s}^{-1}$ (Borkowski & Dwek 1995). The surface binding energy relevant to the grain sputtering is set to be 4 eV, the value typical for amorphous carbon and

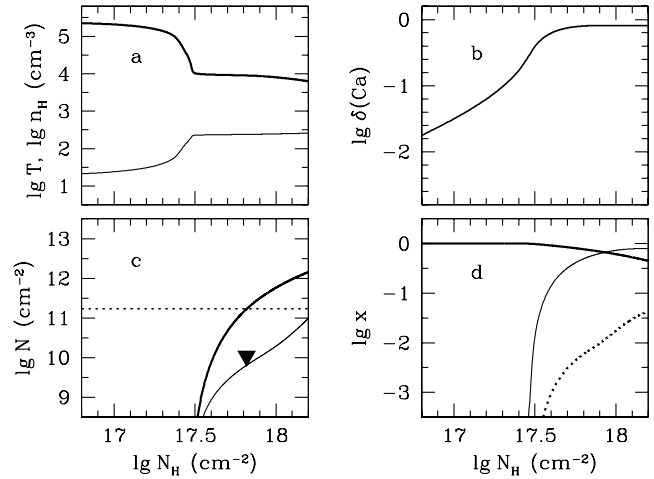


Figure 6. The postshock flow for the shock speed of 140 km s^{-1} as a function of the downstream column density. Shown are (a) temperature (*thick line*) and density; (b) Ca depletion factor; (c) Ca II column density (*thick solid*), Na I column density (*thin solid*), observed Ca II column density (*dotted*), and Na I column density 3σ upper limit (*triangle*); (d) ionization fraction of H (*thick solid*), Ca II (*thin solid*), and Ca I (*dotted*).

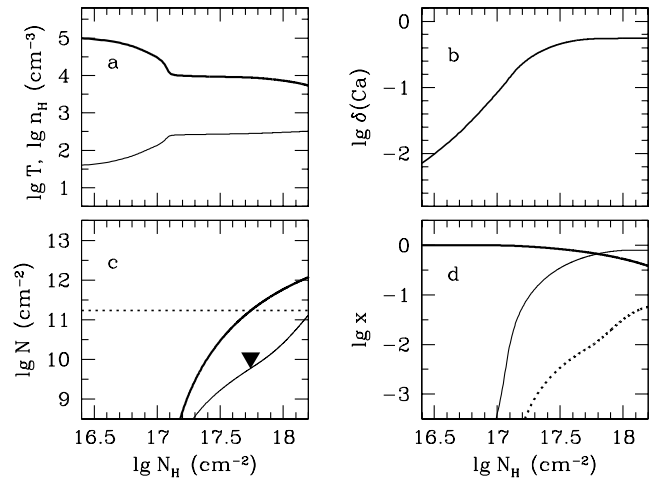


Figure 7. The same as Fig. 6 but for the shock speed of 100 km s^{-1}

iron grains (Tielens et al. 1994). Calcium locked in the dust is assumed to be homogeneously mixed with the grain material.

An approximation of a single grain size with the initial grain radius of 10^{-5} cm is used. The preshock hydrogen ionization fraction is set to $x_0 = 0.1$ and the magnetic field is set to $B_0 = 3 \times 10^{-6}$ G; in fact, results are not very much sensitive to these parameters. In order to estimate the cloud acceleration we adopt the dynamical pressure of the blast wave to be $\rho_c v_s^2$ and the intercloud blast wave speed of 600 km s^{-1} .

4.3 Results of modelling

We focus on the approaching cloud (cloud A) and consider two cases (I) the cloud was shocked recently with the shock speed of 140 km s^{-1} ; (II) the cloud was shocked a long time

ago by the cloud shock with the speed of 100 km s^{-1} and afterwards was accelerated up to 147 km s^{-1} . We have explored an extended parameter space and found an optimal models which meet constraints from both the Ca II column density and acceleration for the case I (Fig. 6). and the case II (Fig. 7).

In case I the observed velocity 147 km s^{-1} is reached in $\approx 20 \text{ yr}$ after the cloud crushing. The optimal value for the cloud preshock density is $n_{c0} = 4 \text{ cm}^{-3}$, while the intercloud density turns out to be $n_{i0} = 0.22 \text{ cm}^{-3}$ assuming $v_b = 600 \text{ km s}^{-1}$. Shown in Fig. 6 as functions of the total hydrogen column density are the temperature, the total hydrogen number density, the Ca depletion parameter, the gaseous Ca II and Na I downstream column density, and the ionization fractions of H, Ca II, and Ca I. The column density of Ca II is sampled primarily in the cooling zone, at about $N_H \sim 4 \times 10^{17} \text{ cm}^{-2}$. The rapid increase of the Ca II density at this distance is an outcome of the density increase in the cooling zone which is followed by the recombination of Ca III into Ca II and the grain destruction. The dominant mechanism of the dust destruction is the non-thermal sputtering due to grain collisions with He atoms and ions. We find that results are robust with respect to the initial depletion factor. The observed Ca II column density for the cloud A is attained in case I at $N_H \sim 6.6 \times 10^{17} \text{ cm}^{-2}$ (Fig. 6c). This can be considered as an estimate of the initial column density of the undisturbed cloud A. The acceleration of the shocked cloud with this column density is $g = 1.2 \times 10^{-3} \text{ cm s}^{-2}$ which coincides within errors with the observed deprojected acceleration of the cloud A. For the adopted cloud column density the radius of the unshocked cloud is $a = 1.2 \times 10^{17} \text{ cm}$ and the cloud crushing time is $t_{cc} = 370 \text{ yr}$. Remarkably, the model Na I column density is consistent with the 3σ upper limit derived from the non-detection of the high-velocity Na I D₂ absorption (Fig. 6c).

In the case II (Fig. 7) the observed Ca II column density and acceleration are satisfied for the total hydrogen column density of $N_H = 5.5 \times 10^{17} \text{ cm}^{-2}$; this value is presumably the column density of cloud A in case II. The cloud number density in this model is $n_{c0} = 6 \text{ cm}^{-3}$ and the intercloud density is $n_{i0} = 0.16 \text{ cm}^{-3}$ assuming $v_b = 600 \text{ km s}^{-1}$. The cloud is crushed at $t_{cc} = 290 \text{ yr}$ while the observed velocity $v_c = 147 \text{ km s}^{-1}$ is attained at $t = 1.4t_{cc} \sim 400 \text{ yr}$. Remarkably, both cases I and II suggest that the shocked cloud is observed at about 400 yr after the interaction began.

The above models demonstrate that for the shock velocity in the range of $100\text{--}140 \text{ km s}^{-1}$ the cloud total hydrogen column density turns out to be in a narrow range of $(5.5\text{--}6.6) \times 10^{17} \text{ cm}^{-2}$. The number density in the undisturbed cloud is in the range of $4\text{--}6 \text{ cm}^{-3}$ with the lower value corresponding to the larger shock velocity, while the cloud radius is in the range of $(0.7\text{--}1.2) \times 10^{17} \text{ cm}^{-2}$ with the lower limit corresponding to the lower shock velocity. If the cloud shape is clumpy, we come to the estimate of the cloud mass in the range of $10^{-3} \text{--} 10^{-2} M_\odot$.

We also have performed simulations for the cloud B and find that the Ca II column density and acceleration are reproduced in cases of high and low cloud shock velocity for the cloud column density in the range of $(4\text{--}5.4) \times 10^{17} \text{ cm}^{-2}$ and cloud number density in the range of $3.8\text{--}5.5 \text{ cm}^{-3}$, both values being similar to those for the cloud A. The fact that both clouds lying at the opposite sides of Vela SNR have

comparable parameters indicates that low column density clouds may be rather common at least for the vicinity of the Vela SNR. We emphasise that this conclusion is rather speculative and requires confirmation by means of similar study of other high-velocity components in Vela SNR.

5 DISCUSSION AND CONCLUSIONS

Our goal was to study the interstellar absorptions in spectra of stars towards RX J0852.0-4622 focusing primarily on the high velocity components associated with shocked clouds. We find that the low velocity absorption components do not show significant anomalies when compared to properties of absorbers in other surveys. The major differences with other surveys are probably caused by the selection effects due to different spectral resolution and S/N ratios.

We find an interesting effect in the distribution of K I absorbers along the distance of background stars towards RX J0852.0-4622: the lack of noticeable K I absorbers at the distances $d < 600 \text{ pc}$ followed by the "jump" of the strength of K I absorbers for $d > 600 \text{ pc}$ which is indicative of the underpopulation of dense clouds at $d < 600 \text{ pc}$. Generally, the distribution of H I gas in external spiral galaxies is intermittent with characteristic scale of several hundred parsecs, which is seen clearly, e.g., in M 51 21 cm map (Rots et al. 1990). It might well be that we look at the RX J0852.0-4622 through such local void with small number of cool clouds. Another possibility is that the hollow in the distribution of K I absorbing clouds might be outcome of the Gum nebula dynamical evolution. Indeed, the Gum supershell is shown to be depopulated by neutral gas clouds between $350\text{--}570 \text{ pc}$ (Woermann et al. 2001).

We have detected four high-velocity ($-v_{lsr} > 100 \text{ km s}^{-1}$) Ca II clouds in spectra of three stars. Towards HD 75309 we see two shocked clouds, both observed earlier in 1993 and 1996 (Cha & Sembach 2000). The large time span of $12\text{--}15 \text{ yr}$ permitted us to detect and measure the acceleration for cloud A and B which turn out to be comparable ($\sim 10^{-3} \text{ cm s}^{-2}$). For the first time the acceleration of shocked clouds is used in combination with the velocity and Ca II column density to recover the cloud total hydrogen column density ($\sim 6 \times 10^{17} \text{ cm}^{-2}$), which implies the cloud radius of $\sim 10^{17} \text{ cm}$ for the estimated cloud density $n_{c0} \sim 5 \text{ cm}^{-3}$. Regardless of our plane shock model is rather crude for the description of a blast wave/cloud interaction we believe that our model grasps the major features of this phenomenon.

The fact that approaching and receding high-velocity clouds on the opposite sides of Vela SNR have comparable parameters indicates that they are possibly rather typical small scale ($a \sim (1\text{--}2) \times 10^{17} \text{ cm}$) clouds in the vicinity of Vela SNR. It is not clear whether all the high-velocity clouds observed in Vela SNR have similar column density but, if we admit they do, it would be instructive to check the outcome of this conjecture. In our sample of 14 stars eleven do not show fast components which translates into the occultation optical depth (average number of clouds on the sight line) $\tau_{oc} = 0.24$. This value is sampled at front and rear sides of the blast wave with the thickness $\Delta R \approx 0.03R$. Adopting the cloud number density distribution $dv/da \propto a^{-3}$ (cf. Appendix A) which follows from the

observed probability density function of HI column density $p(N) \propto N^{-1}$ (Stanimirović & Heiles 2005) and using the estimate $\tau_{oc} = 0.24$ one finds the volume filling factor of clouds with the radii $1 < a_{17} < 2$ to be $f \approx 0.016$. For the cloud total hydrogen density $\sim 5 \text{ cm}^{-3}$ the filling factor of the small size clouds extrapolated to larger sizes should not exceed 0.1 in order to be consistent with the average IS density of $\sim 0.5 \text{ cm}^{-3}$. This means that the upper limit of cloud size for that particular variety is $\sim 4 \times 10^{17} \text{ cm}$. We therefore should admit that either the accelerated clouds are very rare and we catch an improbable chance, or, alternatively, the small-size clouds are rather numerous. If this is the case then possibly this variety of small clouds have not yet been observed. Indeed, if calcium were depleted in these clouds with $\delta = 2 \times 10^{-4}$ then the Ca II column density would not exceed $2 \times 10^8 \text{ cm}^{-2}$ which is below the detection limit. On the other hand, if Ca depletion were moderate, e.g., $\delta \sim 2 \times 10^{-2}$ likewise in clouds studied by Bertin et al. (1993) then the Ca II column density would be as high as $2 \times 10^{10} \text{ cm}^{-2}$ and these clouds could fall in the range of observed thinnest Ca II absorbers.

At a first glance these small clouds could be identified with thin clouds ($N_H \sim 1.3 \times 10^{18} \text{ cm}^{-2}$) revealed by 21 cm absorption (Braun & Kanekar 2005; Stanimirović & Heiles 2005). The problem, however, is that these HI clouds are cool ($T \sim 50 \text{ K}$) and therefore dense ($n(H) \sim 30 \text{ cm}^{-3}$), factor ~ 5 more dense than our clouds. Another problem their low filling factor. Indeed, on the sight line towards 3C286 extragalactic source ($b = 81^\circ$) only three clouds are detected, i.e., the average number of clouds on the sight line $\tau_{oc}=3$. This value is translated into the filling factor f of clouds using the relation

$$\tau_{oc} = \frac{3}{4} \left(\frac{h_z}{a} \right) f, \quad (4)$$

where h_z is HI scale height perpendicular to the Galactic plane, a is the cloud radius. For the typical density of $\sim 30 \text{ cm}^{-3}$ the cloud radius is $a \approx 4 \times 10^{16} \text{ cm}$. Inserting into the equation (4) the values of a , τ_{oc} , and $h_z=100 \text{ pc}$ we get $f \approx 5 \times 10^{-4}$, which is ≈ 30 times smaller than the filling factor of the small clouds around Vela SNR derived assuming that all the high-velocity clouds are small-size clouds. This disparity and larger density of thin 21 cm absorbers imply, that the two varieties of small clouds seem to be different.

Ultraviolet *HST* spectroscopy reveals in the direction $(l, b) \sim (83^\circ, -50^\circ)$ a cloud with the column density of $N_H \sim 6 \times 10^{17} \text{ cm}^{-2}$ and number density of $20\text{--}45 \text{ cm}^{-3}$ (Welty 2007). Again, this cloud has comparable column density with our A and B clouds but the number density is of one order magnitude larger. In fact, the density of A and B clouds ($\sim 5 \text{ cm}^{-3}$) is somewhat unusual: it falls into unstable region of phase diagram for the typical pressure $P/k \approx 3000 \text{ cm}^{-3} \text{ K}$ (Wolfire et al. 2003). This means that either A and B cloud were in the unstable state, or the pressure in the vicinity of Vela SNR is significantly (one order of magnitude) larger than the typical pressure. The latter, however, seems less likely because according to the extensive survey of UV fine-structure C I absorption lines the typical pressure lies in the range $10^3 \lesssim P/k \lesssim 10^4$ (Jenkins & Tripp 2001).

To conclude, the detection of the acceleration of two shocked clouds in Vela SNR along the same sight line and the fact of similarity of their parameters are exciting re-

sults which might have interesting implications for our understanding of cloudy structure of the ISM at small scales of $\sim 10^{17} \text{ cm}$. However, the issue, whether these clouds are common for diffuse ISM, or we observe highly improbable event, remains to be explored, e.g., by means of the study the velocity evolution of other high-velocity absorbing clouds in Vela SNR.

6 ACKNOWLEDGEMENTS

This study is partially supported by the Program of State Support to Leading Scientific Schools of the Russian Federation (grant 3602.2012.2) and by the Basic Research Program of the Russian Academy of Sciences “Nonstationary phenomena in the Universe”.

APPENDIX A: RELATION BETWEEN OBSERVED AND TRUE DISTRIBUTION OF CLOUD SIZES

We consider homogeneous spatial distribution of spherical clouds of the same density. A line segment of a length L produced by a random sight line can be considered as a proxy for the corresponding column density N . The probability density function of segments for a cloud of the radius a is $p(L, a) = (1/2)L/a^2$. Let the true cloud number density distribution of cloud radii be $dn/da = Ca^{-\gamma}$, while $dn/dN \propto dn/dL$ is the observed column density (or segment) distribution per unit length along some line of sight. We then have an obvious relation between dn/da and dn/dL

$$dn/dL = \int_{L/2}^{a_{\max}} \pi a^2 (dn/da) p(L, a) da \propto L^{-(\gamma-2)},$$

where we assume that $\gamma > 2$ and $a_{\max} \gg L$. For the case $dn/dN \propto N^{-1}$ suggested by 21 cm observations (Stanimirović & Heiles 2005) one gets $\gamma = 3$.

REFERENCES

- Aschenbach B., 1998, *Nature*, 396, 141
- Bertin P., Lallement R., Ferlet R., Vidal-Madjar A., 1993, *A&A*, 278, 549
- Bocchino F., Maggio A., Sciortino S., 1999, *A&A*, 342, 839
- Borkowski K. J., Dwek E., 1995, *ApJ*, 454, 254
- Braun R., Kanekar N., 2005, *A&A*, 436, L53
- Cha A. N., Sembach K. R., 2000, *ApJS*, 126, 399
- Cha A. N., Sembach K. R., Danks A. C., 1999, *ApJ*, 515, L25
- Cox D. P., 1972, *ApJ*, 178, 143
- Crawford I. A., 2001, *MNRAS*, 328, 1115
- Crawford I. A., 2003, *Ap&SS*, 285, 661
- Danks A. C., Sembach K. R., 1995, *AJ*, 109, 2627
- Draine B. T., Salpeter E. E., 1979, *ApJ*, 231, 77
- Famaey B., Jorissen A., Luri X., Mayor M., Udry S., Dejonghe H., Turon C., 2005, *A&A*, 430, 165
- Friedman S. D., York D. G., McCall B. J., Dahlstrom J., Sonnentrucker P., Welty D. E., Drosbach M. M., Hobbs L. M., Rachford B. L., Snow T. P., 2011, *ApJ*, 727, 33
- Gredel R., van Dishoeck E. F., Black J. H., 1993, *A&A*, 269, 477

- Iyudin A. F., Pakhomov Y. V., Chugai N. N., Greiner J., Axelsson M., Larsson S., Ryabchikova T. A., 2010, *A&A*, 519, A86+
- Iyudin A. F., Schönfelder V., Bennett K., Bloemen H., Diehl R., Hermsen W., Lichti G. G., van der Meulen R. D., Ryan J., Winkler C., 1998, *Nature*, 396, 142
- Jenkins E. B., Tripp T. M., 2001, *ApJS*, 137, 297
- Jenkins E. B., Wallerstein G., Silk J., 1976, *ApJ*, 209, L87
- Jura M., Dalgarno A., 1972, *ApJ*, 174, 365
- Klein R. I., McKee C. F., Colella P., 1994, *ApJ*, 420, 213
- Kritsuk A. G., Ustyugov S. D., Norman M. L., 2011, in Alves J., Elmegreen B. G., Girart J. M., Trimble V., eds, *Computational Star Formation Vol. 270 of IAU Symposium, Interstellar Turbulence and Star Formation*. pp 179–186
- Kupka F., Piskunov N., Ryabchikova T. A., Stempels H. C., Weiss W. W., 1999, *A&AS*, 138, 119
- Kurucz R., , 1993, *ATLAS9 Stellar Atmosphere Programs and 2 km/s grid*. Kurucz CD-ROM No. 13. Cambridge, Mass.: Smithsonian Astrophysical Observatory, 1993.
- McKee C. F., Hollenbach D. J., Seab G. C., Tielens A. G. G. M., 1987, *ApJ*, 318, 674
- Patnaude D. J., Fesen R. A., 2005, *ApJ*, 633, 240
- Rots A. H., Bosma A., van der Hulst J. M., Athanassoula E., Crane P. C., 1990, *AJ*, 100, 387
- Routly P. M., Spitzer Jr. L., 1952, *ApJ*, 115, 227
- Savage B. D., Sembach K. R., 1996, *ApJ*, 470, 893
- Shull J. M., 1977, *ApJ*, 215, 805
- Stanimirović S., Heiles C., 2005, *ApJ*, 631, 371
- Sutherland R. S., Dopita M. A., 1993, *ApJS*, 88, 253
- Tielens A. G. G. M., McKee C. F., Seab C. G., Hollenbach D. J., 1994, *ApJ*, 431, 321
- Tsymbal V., Lyashko D., Weiss W. W., 2003, in N. Piskunov, W. W. Weiss, & D. F. Gray ed., *Modelling of Stellar Atmospheres Vol. 210 of IAU Symposium, Processing Stellar Echelle Spectra*. pp 49P–+
- Wallerstein G., Silk J., 1971, *ApJ*, 170, 289
- Welty D. E., 2007, *ApJ*, 668, 1012
- Welty D. E., Hobbs L. M., 2001, *ApJS*, 133, 345
- Welty D. E., Hobbs L. M., Kulkarni V. P., 1994, *ApJ*, 436, 152
- Welty D. E., Hobbs L. M., Morton D. C., 2003, *ApJS*, 147, 61
- Woermann B., Gaylard M. J., Otrupcek R., 2001, *MNRAS*, 325, 1213
- Wolfire M. G., Hollenbach D., McKee C. F., Tielens A. G. G. M., Bakes E. L. O., 1995, *ApJ*, 443, 152
- Wolfire M. G., McKee C. F., Hollenbach D., Tielens A. G. G. M., 2003, *ApJ*, 587, 278